The Nuclearity of the Active Site for Methane to Methanol Conversion in Cu-Mordenite: A Quantitative Assessment

The nuclearity of the active site for methane to methanol conversion in Cu-mordenite: a quantitative assessment

Dimitrios K. Pappas[1], Andrea Martini[2,3], Michael Dyballa[1,4‡], Karoline Kvande[1], Shewangizaw Teketel[5], Kirill A. Lomachenko[6], Rafal Baran[6], Pieter Glatzel[6], Bjørnar Arstad[4], Gloria Berlier[2], Carlo Lamberti[3,7], Silvia Bordiga[1,2], Unni Olsbye[1], Stian Svelle[1*], Pablo Beato[5*], Elisa Borfecchia[2,5*†]

[1]Center for Materials Science and Nanotechnology (SMN), Department of Chemistry, University of Oslo, 1033 Blindern, 0315 Oslo, Norway

[2]Department of Chemistry and INSTM Reference Center, University of Turin, via P. Giuria 7, 10125 Turin, Italy

[3]IRC "Smart Materials", Southern Federal University, Zorge Street 5, 344090 Rostov-on-Don, Russia

[4]SINTEF Industry, Forskningsveien 1, 0373 Oslo, Norway

[5]Haldor Topsøe A/S, Haldor Topsøes Allé 1, 2800 Kongens Lyngby, Denmark

[6]European Synchrotron Radiation Facility (ESRF), 71 avenue des Martyrs, CS 40220, 38043 Grenoble Cedex 9, France

[7]Department of Physics, University of Turin, via P. Giuria 1, 10125 Turin, Italy

ABSTRACT: The direct conversion of methane to methanol (MTM) is a reaction which has the potential to disrupt great part of the synthesis gas derived chemical industry. However, despite many decades of research, active enough catalysts and suitable processes for industrial application are still not available. Recently, several copper-exchanged zeolites have shown considerable activity and selectivity in the direct MTM reaction. Understanding the nature of the active site in these materials is essential for any further development in the field. Herein, we apply multivariate curve resolution analysis of X-ray absorption spectroscopy (XAS) data to accurately quantify the fraction of active Cu in Cu-MOR, allowing an unambiguous determination of the active site nuclearity as a di-copper site. By rationalizing the compositional parameters and reaction conditions, we achieve the highest methanol yield per Cu yet reported for MTM over Cu-zeolites, of 0.47 mol/mol.

1. Introduction

The global stock of methane from shale gas, hydrates and coalbed methane is constantly increasing[1] but the transportation and processing are challenging.[2] Routes which can transform methane to high value chemicals directly, avoiding the highly energy-consuming syngas route are therefore economically and environmentally desirable. Reactive coupling of methane enables the direct production of olefins and aromatics in a high temperature operation.[3] Direct oxidation of methane requires milder conditions, but suffers from both low conversion and selectivity or involves costly oxidants.[2, 4-5] Inspired by methanotrophic enzymes with copper in active complexes,[6] researchers were able to mimic the sites that are found in nature in the confined environment of zeolite pores.[7-8] The resulting materials are able to cleave the C-H bond and stabilize a methyl-group which is later hydrolyzed into methanol.[9] Until now, different zeolite frameworks (i.e., MFI,[7, 10] MOR[9, 11-14] and CHA[15-16]) have been demonstrated to stabilize Cu in active sites (AS). The direct conversion of methane to methanol (MTM) over these materials involves three consecutive steps: high temperature activation in O_2, CH_4 loading at 200 °C and finally extraction of the products with steam.

The MOR structure has straight twelve membered ring pores (12MR) (7.0 × 6.5 Å), interconnected by 8MR channels (5.7 × 2.6 Å) that are very narrow in one place, leading to what can more precisely be described as the 8MR side pockets. Cu is preferentially exchanged into these side pockets where it balances the framework charge, forming active Cu_xO_y species upon activation in O_2[12-13, 17-18] The exact nature and diversity of Cu-centres formed during high-temperature oxidative treatment is still under debate. To date, dinuclear[9, 19-23] or trinuclear[13] Cu-oxo

species have been proposed as the most favorable AS for methane activation. Recently, the effect of the aluminum content in the MOR framework was addressed leading to the conclusion that both monomeric as well as dimeric Cu-species can be present and active for the conversion.[24] It appears that the speciation of Cu in MOR goes beyond the single-site paradigm, and that it can be dynamically transformed, influenced by composition as well as by synthesis and pre-treatment conditions, as demonstrated for the CHA framework.[16, 25-26]

Herein, we evaluated Cu-MOR zeolites of different composition for the MTM conversion. The normalized product yields per Cu indicate a uniform population of active sites, with the exception of one sample, where the maximum stoichiometry of a di-copper AS – of almost 0.5 mol CH_3OH/mol Cu, is reached. Aiming to rationalize this unique behaviour, we exploited X-ray Absorption Spectroscopy (XAS) to shed light on the nature of Cu ions in the MOR zeolite. The subtle differences between active and inactive Cu^{II} species formed during O_2-activation call for advanced experimental and analytical approaches, to add species-sensitivity to the absorbing-atom-averaged XAS response. Additionally, the duration of the key reaction steps is observed to largely impact the product yield, requiring the use of consistent reaction conditions for spectroscopy and testing. Having fulfilled these requirements, we show how Multivariate Curve Resolution (MCR) analysis of *in situ* High-Energy-Resolution Fluorescence-Detected (HERFD) XANES can enable an accurate quantification of the fraction of active Cu in O_2-activated Cu-MOR, allowing an unbiased and unequivocal determination of the AS nuclearity as a di-copper site.

2. METHODS

2.1. Cu-MOR synthesis and physico-chemical characterization.

Commercial zeolites CBV21A (NH_4-MOR, Si/Al=11) and CBV10ADS (Na-MOR, Si/Al=7) from Zeolyst Inc. were utilized as parent materials. The first was once and the latter was three times ion exchanged with NH_4NO_3 (10 wt% in water) at 60 °C for 5 h. Both were washed NO_3-free; no Na was detected by EDX. NH_3 was burned off by heating (1 °C /min) in air at 500 °C for 8 h, afterwards the resulting H-form zeolites were cooled to room temperature (RT), slowly re-hydrated in air and then exchanged. Aqueous solutions (60 ml/g) of copper(II) acetate (99.99%, Sigma-Aldrich) with 0.005 to 0.02 M were utilized for the exchange which was conducted under stirring at RT overnight. The pH was adjusted during the exchange, with NH_4OH-solution (28%, Sigma-Aldrich) and 0.1 M HNO_3, between 5.2 and 5.7. After exchange, the materials were washed three times with water in order to remove excess copper ions and avoid overloading. Standard physico-chemical analysis of all the investigated materials was carried out by XRD, SEM-EDX, N_2-physisorption and ^{27}Al MAS NMR spectroscopy as described in Supporting Information (SI), Section S1.

2.2. Testing for MTM conversion over Cu-MOR.

Cu-MOR zeolites were evaluated with respect to the activity towards MTM conversion in a quartz plug flow reactor (I.D. =6 mm). The temperature was controlled by a tubular oven monitored by a thermocouple placed in the centre of the bed. For each measurement 100 mg of powder was utilized. Prior the sample was pressed in pellets, ground and sieved in order to obtain uniform particles in the 250 to 425 μm range. The stepwise MTM process included the following three steps: (i) activation in oxygen at high temperature; (ii) reaction with methane; (iii) extraction of methanol with steam. Between each step the materials were flushed with He. In the reference testing conditions, the Cu-MOR powder was initially dried in He flow (15 ml/min) at 150 °C; afterwards an O_2 flow (15 ml/min) was introduced and the temperature increased with 5 °C/min to 500 °C, where it stayed for 480 min. After activation, the temperature was decreased to 200 °C with a rate of 5 °C/min in O_2. The sample was then purged with He for 60 min before CH_4 loading step; 15 ml/min CH_4 flow for 360 minutes at 200 °C. After the loading step, the sample was purged again and online H_2O-assisted extraction of CH_3OH was performed isothermally. A flow of Ne/He (13.5 ml/min) was passed through a saturator containing deionized water at 44 °C. After the purging step, the steam was introduced to the sample and the effluent was analysed by a Hewlett Packard 6890/5972 GCMS System. This protocol was repeated using shorter O_2-activation and CH_4 loading steps in the *operando* XAS testing conditions and in the HERFD XANES testing conditions (see SI, Section S2 for a detailed overview).

2.3. Operando XAS.

Operando XAS experiments were performed at the BM31 beamline (Swiss Norwegian Beamline, SNBL) of the European Synchrotron Radiation Facility (ESRF, Grenoble, France). We collected Cu K-edge XAS spectra in transmission mode, using a water-cooled flat Si [111] double crystal monochromator. To measure the incident (I_0) and transmitted (I_1) X-ray intensity, 30 cm-length ionization chambers filled with a mixture of He and Ar were used. Continuous scans were performed in the 8800–10000 eV range, with a constant energy step of 0.5 eV. Collection of one XAS spectrum required 10 min. We characterized the O_2-activated state for each material collecting two consecutive scans and averaging the corresponding μ(E) curves after checking for signal reproducibility. For the measurements, the Cu-MOR powder was ground and sieved with 250 to 212 μm sieves; ca. 3 mg of powder was then packed in a capillary reactor (1 mm diameter) connected to an appropriate gas-flow setup for the stepwise MTM reaction. Temperature at the measurement position was controlled by a heat gun. A total flow rate of 2 ml/min was employed for all the reaction steps, including O_2-activation at 500 °C in pure O_2 (90 min), pure CH_4 loading at 200 °C (120 min), and CH_3OH extraction by steam admission at 200 °C (70 min). The heating and cooling ramps were always performed using a rate of +/– 5 °C/min. For the extraction step, a flow of Ne/He was passed through a saturator containing deionized water at 44 °C. The steam was then introduced to the sample and the effluent was analysed by a quadrupole MS (Pfeiffer Vacuum), to quantity the productivity for investigated samples at the *operando* XAS conditions. XAS spectra were normalized to unity edge jump using the Athena software from the Demeter package.[27] The extraction of the χ(k) EXAFS functions was also performed using Athena program and R-space EXAFS spectra were obtained by calculating the Fourier transform of the $k^2\chi(k)$ functions in the (2.4 – 8.7) $Å^{-1}$ k-range.

2.4. In situ HERFD XANES.

HERFD XANES measurements were performed at the ID26 beamline of the ESRF. The spectra were acquired in fluorescence mode, detecting only photons whose energy corresponded to the maximum intensity of the Cu $K_{\beta1,3}$ emission line (~8906 eV). This energy selection was performed using five Si [553] analyser crystals (θ = 79.92°), set up in vertical Rowland geometry, resulting in spectra resolution of 1.06 eV (elastic peak). The crystals were spherically bent following the Johann scheme to focus the fluorescence radiation onto an APD detector. For the incident beam a flat double-crystal Si [311] monochromator was employed. The time acquisition for each spectrum was set to 2 min.

The measurements were conducted using a well-established gas-flow setup, based on the Microtomo reactor cell (developed by the ESRF Sample Environment team),[28] that allowed to precisely control the gas composition and the temperature inside, as described in details in our previous works.[29-30] The Cu-MOR samples were prepared in the form of self-supporting wafers (ca. 100 mg of sample) and fixed inside the reactor cell. *In situ* experiments during He- and O_2-activation were performed heating the samples from 60 °C to 500 °C with a heating ramp of 5 °C/min and flowing in the Microtomo reactor cell 100 ml/min gas He or O_2, depending on the type of pre-treatment. The evolution of the XANES during the temperature ramp was continuously monitored by 2 min scans. After the samples were kept 30 min at 500 °C in He or in O_2, 5 additional scans were collected and averaged to obtain a higher-quality HERFD XANES spectrum. In addition, for the two Si/Al = 7 samples, a He-activated + O_2 state was characterized. The samples were kept at 500 °C in He for 240 min, and subsequently exposed to pure O_2 at the same temperature; five HERFD XANES were collected after 120 or 150 min in O_2 at 500 °C, for 0.18Cu-HMOR(7) and 0.24Cu-HMOR(7), respectively, and then averaged as described before. All the collected HERFD XANES spectra were normalized to unity edge jump using the Athena software from the Demeter package.[27]

2.5 MCR-ALS analysis.

Multivariate Curve Resolution (MCR) is an emerging data analysis technique, allowing to model an experimental dataset $\mathbf{D}$ (including q spectra), as the product of a $\mathbf{S}$ matrix, composed by N (with $N < q$) pure spectra and a matrix $\mathbf{C}$ which elements correspond to signal-related concentration profiles: $\mathbf{D} = \mathbf{C}\,\mathbf{S}^T + \mathbf{E}$, where $\mathbf{S}^T$ is the transpose of matrix $\mathbf{S}$, while $\mathbf{E}$ represents the error matrix associated to the reconstruction. To this aim, the Multivariate Curve Resolution Alternating Least Squares (MCR-ALS) algorithm employed in this work performs the dissociation

optimizing concentration profiles and pure spectra in an altering least square under constraints.[31-33] The first step of the algorithm requires the determination of the number of statistically significant components in the experimental data matrix. To this purpose, we performed Principal Component Analysis (PCA).[34] As described in the SI, Section S8, PCA indicated five principal components in the dataset reported in Figure 3a. For MCR-ALS analysis we employed the Graphical User Interface (GUI) by Jaumot and co-workers,[35] freely downloadable at http://www.mcrals.info/, using Matlab R2011b. The analysed dataset globally consisted in a column-wise augmented matrix obtained by joining the four HERFD XANES datasets collected on 0.18Cu-HMOR(7) and 0.36Cu-HMOR(11) during O_2-activation and He-activation (45 scans for each sub-dataset, 180 scans in total). For MCR, the spectra were analysed in the 8975−9021 eV energy range, including 460 energy points. The initial un-mixing data procedure was performed using the SIMPLISMA algorithm,[36] with an allowed noise parameter fixed at 5%.[31] The ALS routine was run employing the following *soft* constraints: non-negativity for both pure spectra and concentration profiles (using the fast non-negative least squares algorithm, *fnnl*[37]) and closure to 1 for the concentration profiles (permitted since an element-selective technique is employed, probing all the Cu in the system). The optimization routine successfully converged after 20 iterations, resulting in the final ALS quality control parameters shown in the SI, Table S7.

3. Results

3.1. Composition-productivity trends for MTM over Cu-MOR

Cu-exchanged mordenites (Cu-MOR) were synthesized via liquid ion exchange of the parent H-form (HMOR, Si/Al=11 and Si/Al=7) and denoted as xCu-HMOR(y) where x and y represent the Cu/Al and Si/Al ratios, respectively. Microscopy reveals partially agglomerated crystals in the range of 50 to 300 nm, without detectable Cu nanoparticles. Additional details on the synthesis as well as the physico-chemical characterization of the parent and Cu-exchanged mordenite zeolites can be found in the Methods as well as in the SI.

The synthesized Cu-MOR zeolites were evaluated for their activity in the MTM reaction. The samples were first activated at 500 °C in O_2 flow for 480 min then reacted with CH_4 at 200 °C for 360 min (Figure 1a); finally, the products were extracted with steam isothermally and analysed by an online Mass Spectrometer (MS), see also Methods and SI, Section S2. The methanol output is illustrated in Figure 1b-c as yield per gram of sample (μmol/g) as well as normalized by Cu content (mol/mol, Figure 1d). The Cu-MOR samples with Si/Al=11 exhibit a linear trend of the yield with increasing Cu loading, reflected in an almost constant normalized productivity (ca 0.25 mol/mol). A similar behaviour is exhibited by the materials with Si/Al=7 having the lowest and the highest Cu-loading in the series. These findings are in line with previous reports for Cu-MOR. Here, the density of active sites is mostly found proportional to the Cu concentration, translating into a similar normalized productivity/selectivity for materials with the same Si/Al ratio and indicating a uniform nature of the AS throughout the compositional space.[12-13]

However, the material with intermediate Cu loading (Cu/Al=0.18) exhibits an outstanding performance, yielding 170 μmol/g_{cat}. The nuclearity of the AS reported for similar Cu-MOR materials has been proposed to vary from two to three Cu atoms. From the data reported in Figure 1, it appears that the 0.18Cu-HMOR(7) sample, with a normalized productivity of ca. 0.47 mol/mol, performs close to the maximum value allowed by the stoichiometry assuming a di-copper AS, exhibiting a uniquely high density of active species.

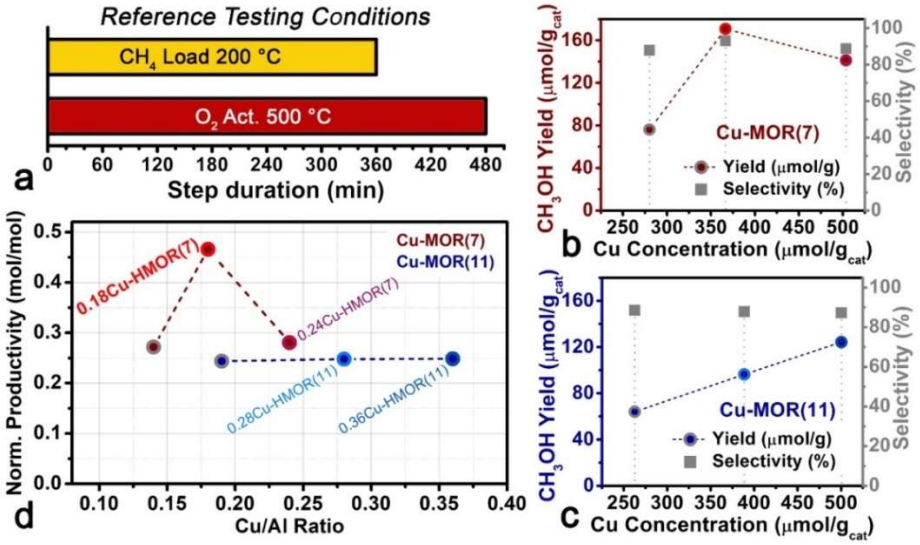

Figure 1. a, Bar plot representing the duration of the O_2-activation and CH_4 loading steps at the reference testing conditions adopted to obtain the productivity values reported in the figure. For detailed reaction conditions, see Methods and SI, Section S2. b, c, CH_3OH yield (μmol $CH_3OH/g_{cat,}$ coloured circles, left ordinate axis) and selectivity (%, grey squares, right ordinate axis) as a function of Cu concentration (μmol Cu/g_{cat}) for Cu-MOR materials with Si/Al = 7 (b, Cu-MOR(7) series) and Si/Al = 11 (c, Cu-MOR(11) series). d, Normalized productivity (mol CH_3OH/mol Cu) as a function of the Cu/Al ratio, comparing the Cu-MOR(7) and the Cu-MOR(11) series. The four samples selected for spectroscopic characterization are highlighted with coloured contours, using the same colour code as in the following figures.

It should be emphasized that the performance of this material was fully reproducible, also when starting with the introduction of Cu into the same zeolite (see Figure S4 in the SI). To assess the impact of the zeolite synthesis on the outstanding performance of 0.18Cu-HMOR(7), we synthesized *ex novo* a Cu-MOR zeolite in house, targeting the same composition (Si/Al = 7 and Cu/Al=0.18). Our efforts resulted in the 0.20Cu-HMOR(7)_*en* sample with Si/Al = 7 and Cu/Al = 0.20. As reported in the SI (Section S4), the newly prepared material at the reference MTM testing conditions gives a normalized CH_3OH yield of 0.19 mol/mol, not comparable with the performance of 0.18Cu-HMOR(7). Taken together, these results indicate an optimum combination of zeolite synthesis parameters, Si/Al ratio (both key factors in determining the framework Al distribution) and Cu-loading with respect to methanol yield. Nonetheless, to determine the exact fraction of active Cu over total Cu, the AS nuclearity needs to be independently proven, while linking the singular performance of 0.18Cu-HMOR(7) to an atomic-scale understanding of Cu-speciation across the compositional series.

3.2 Cu active site spectroscopic fingerprints from operando XAS

To rationalize the composition-productivity trends highlighted above, we initially applied *operando* XAS at the Cu K-edge. We selected two representative materials for each Si/Al ratio, namely 0.18Cu-, 0.24Cu-HMOR(7) and 0.28Cu-, 0.36Cu-HMOR(11). Using a capillary reactor, we performed the MTM reaction cycle over each material, while monitoring the average electronic and structural properties of the Cu ions by XAS (see also Methods).

The methane-converting Cu sites are formed during the high-temperature activation step in an oxidizing atmosphere.[16, 38] Hence, we focus on the comparison of the X-ray Absorption Near Edge Structure (XANES) and Extended X-ray Absorption Fine Structure (EXAFS) spectra of the O_2-activated materials, reported in Figure 2a and Figure 2b, c respectively.

The XANES features can be interpreted based on previous studies on Cu-MOR[13, 20] and other Cu-zeolites.[16, 25, 29-30, 39] For all the samples, O_2-activation results in a virtually pure Cu^{II} state; no Cu^{I} contribution is observed within the detection limit. The XANES spectra of the four Cu-MOR zeolites show remarkable similarities, thus revealing comparable coordination environments for the Cu ions in the pores. Nonetheless, a trend is observed in the intensity of the so-called White-Line (WL) peak at ca. 9000 eV in the XANES (faded grey arrow in the inset of Figure 2a).

Low Si/Al and low Cu/Al both appear to promote a higher WL intensity, with the outperforming 0.18Cu-HMOR(7) showing the highest WL peak.

A higher WL intensity in Cu K-edge XANES is commonly associated with a higher coordination number in the first shell of the cation, as well as to a more uniform bond length distribution. The Fourier Transform (FT) EXAFS spectra in Figure 2b, c confirm this observation. The intensity of the first-shell peak, stemming from scattering contributions by framework (O_{fw}) and extra-framework (O_{ef}) oxygen atoms, follows the same trend. The EXAFS for the four materials also shows a well-defined peak in the second-shell region, extending from 2 to 3 Å in the phase-uncorrected spectra. Guided by previous studies,[16, 20, 25, 30, 39] we expect both Al and Si atoms belonging to the framework (T_{fw}) and Cu–Cu scattering from Cu_xO_y multimeric moieties to contribute in this R-space range. Notably, this peak undergoes intensity modifications as a function of the composition (insets of Figure 2b, faded grey arrow). 0.18Cu-HMOR(7) displays the highest intensity, followed by 0.24Cu-HMOR(7) and then by the two Si/Al=11 samples. The latter show an equivalent development of the EXAFS features in this R-space range.

After 90 min in O_2 at 500 °C, the samples were cooled down to 200 °C and reacted with methane for 120 min. MS analysis of the reactor effluent during the steam-assisted CH_3OH extraction (see also SI, Section 5.2) allowed for on-line quantification of the yield. Figure 2e compares the normalized productivity evaluated under the *operando* XAS conditions (Figure 2d) as well as under the reference testing conditions (Figure 1a). The results demonstrate that our materials were active under the XAS conditions, although the normalized productivity is on average (71 ± 1) % lower compared to the reference conditions. This decrease points out how the duration of the key reaction steps affect the methanol yield,[16] while exactly the same activity trend is maintained.

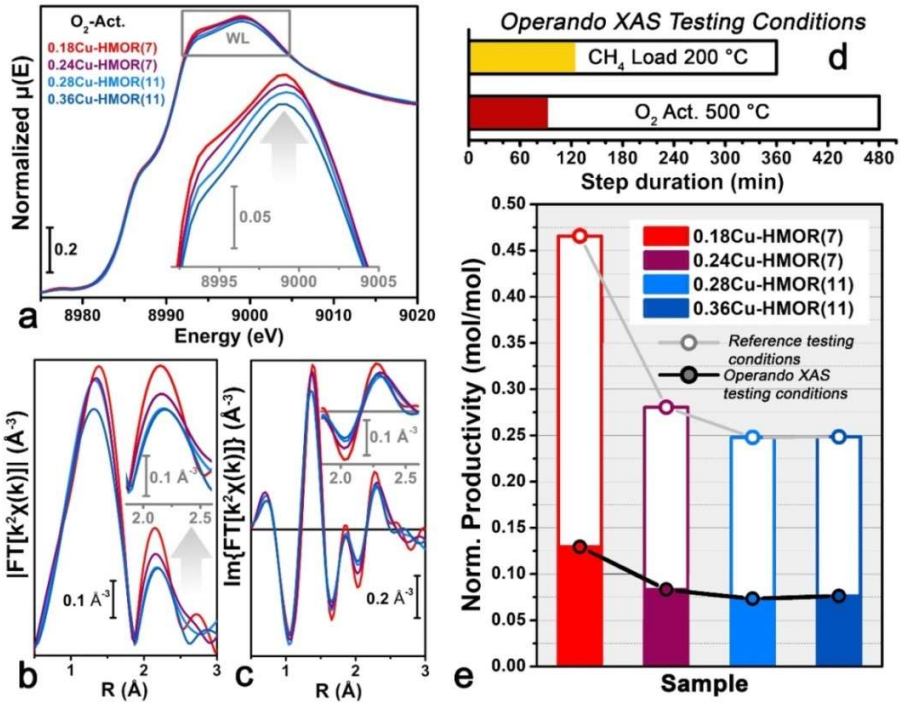

Figure 2. a, Normalized Cu K-edge XANES spectra of selected Cu-MOR samples after O_2-activation at 500 °C. The inset reports a magnification of the so-called white-line (WL) peak, highlighted by the grey box in the main panel. b, c, Magnitude (b) and imaginary part (c) of the corresponding phase-uncorrected FT-EXAFS spectra. The insets in both part b and c report a magnification of the second-shell peak. d, Bar plot comparing the duration of the O_2-activation and CH_4 loading steps under the *operando* XAS (coloured portion of the bars) and the reference conditions. e, Corresponding normalized productivity at the *operando* XAS conditions (full coloured bars and circles) in comparison with the reference testing conditions (empty bars and circles). In all the panels, the same colour code is used to identify the different investigated materials.

Intriguingly, the normalized productivity directly correlates with the intensity of the second-shell peak in the EXAFS spectra. A higher second-shell peak associates with a higher fraction of active Cu in the materials. Cu–T_{fw}

scattering contributions are expected to be equally present into both monomeric and multimeric Cu^{II} moieties coordinated to O_{fw} atoms at well-defined exchange sites in the zeolite framework (fw-Cu^{II}) and we attribute the increased intensity to a stronger Cu–Cu contribution. EXAFS thus provides direct structural evidence for multi-copper active sites in Cu-MOR. Nonetheless, the relatively low abundance of active species formed at the XAS conditions, together with the limited contrast between the spectral signatures of active and inactive Cu^{II}, hampers the quantification of the fraction of active Cu from the *operando* XAS data in Figure 2.

3.3. Enhancing the spectroscopic contrast by MCR analysis of HERFD XANES

Aiming at a quantitative understanding of the structure-activity relationships for Cu-MOR, we measured sequences of HERFD XANES spectra during high-temperature treatment in O_2 and He gas flow for 0.18Cu-HMOR(7) and 0.36Cu-HMOR(11) (see Methods for experimental details). Indeed, monitoring the resistance of different fw-Cu^{II} species to the so-called self-reduction (well known to occur in Cu-zeolites during thermal treatment in inert conditions[20, 30, 40-42]) can assist their identification.[25, 43] In parallel, the higher energy resolution, ensured by using an X-ray spectrometer,[44-45] was crucial to successfully resolve the XANES of active and inactive Cu.

Figure 3 displays the evolution of the HERFD XANES for the two Cu-MOR samples as a function of the temperature, from 60 to 500 °C. The XANES evolution up to ca. 250 °C is only weakly affected by the gaseous environment. All the observed spectral modifications in this temperature window are consistent with thermally-driven dehydration of the Cu centers.[20, 30, 43] However, at higher temperatures, the pre-treatment environment drastically impacts the XANES features, resulting in distinct O_2- and He-activated final states. The HERFD XANES spectra at 500 °C in O_2 match the corresponding conventional XANES in Figure 2a, indicating a dominant contribution from fw-Cu^{II} species. Considerably more defined peaks are observed, in line with the better detection scheme. In contrast, a substantial population of Cu^{I} species is detected at 500 °C in He. The intense peak developing at 8983 eV points to quasi-linear Cu^{I} configurations,[46] in line with earlier observations for Cu-MOR[19] and Cu-MFI.[47]

Similar XANES features are well documented to develop during interaction of O_2-activated Cu-zeolites with CH_4, resulting in the formation of Cu^{I} ions.[9, 13, 16, 21, 48] In this respect, Netwon et al.[48] have recently evaluated by Cu K-edge XANES the fraction of Cu^{I} formed during the CH_4-loading step of the MTM process over various Cu-zeolites. The results are correlated to the methanol yield, as determined by independent reactor-based tests. Therein, the authors highlight a general relationship between the fraction of Cu^{I} and the methanol productivity, consistent with a two-electron CH_4 conversion mechanism based on Cu^{II}/Cu^{I} redox couples. Hereafter, we will look the problem from a different angle, i.e. determining and correlating with the productivity per Cu the fraction of active Cu species formed during O_2-activation, to quantitatively assess the AS nuclearity.

Notably, the outperforming 0.18Cu-HMOR(7) appears to be more resistant to self-reduction compared to 0.36Cu-HMOR(11). Indeed, it shows an almost halved intensity of the Cu^{I} peak at 8983 eV, a significantly higher Cu^{II} 1s→3d pre-edge peak and a WL peak more similar to what is otherwise observed after O_2-activation. We employed statistical analysis and Multivariate Curve Resolution (MCR) on the large HERFD XANES dataset in Figure 3a to resolve the spectra and concentration profiles of the Cu-species formed in the two Cu-MOR samples as a function of temperature and activation conditions. Principal component analysis (PCA, see SI, Section 8.1) indicated that the whole dataset can be described by linear combinations of the spectra of five Cu species. The actual spectra of the five Cu species were obtained by a MCR algorithm, as detailed in the Methods. The MCR results are summarized in Figure 3b,c reporting the theoretical HERFD XANES spectra and their concentration profiles for the tested material/activation protocols combinations.

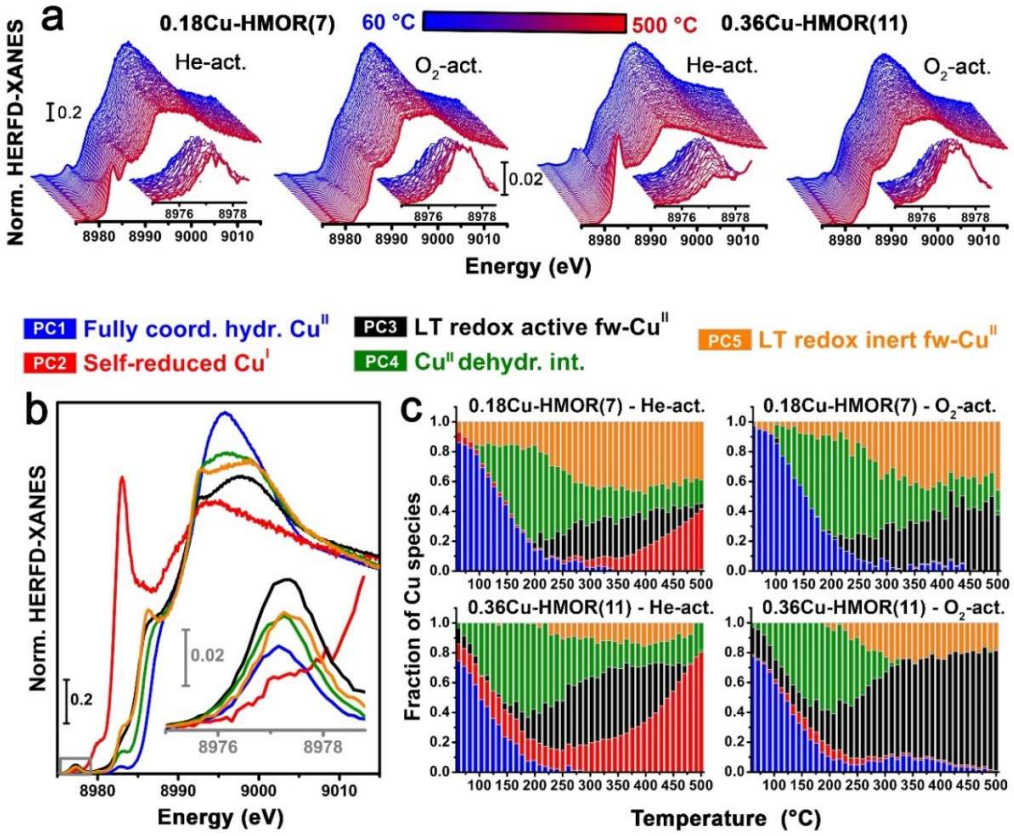

Figure 3. a, Time-dependent HERFD XANES collected on 0.18Cu-HMOR(7), left panels, and 0.36Cu-HMOR(11), right panels, during thermal treatment in O_2 and He gas flow from 60 °C (blue curves) to 500 °C (red curves), using an heating rate of 5 °C/min (ca. 90 min for each experiment). The insets report a magnification of the weak pre-edge peak mostly deriving from the dipole forbidden 1s→3d transition in d^9 Cu^{II} centers. **b,** Theoretical 'pure' HERFD XANES spectra of Cu-species from MCR analysis of the dataset in part **a**. **c**, Corresponding temperature-dependent concentration profiles of each Cu-species. In a similar way as recently found for Cu-CHA,[43] pseudo-octahedral Cu^{II} aquo complexes (**PC1**) undergoes partial dehydration to four-coordinated Cu^{II} species (**PC4**). These Cu^{II} dehydration intermediates reach maximum concentration around 200 °C, and then progressively convert into framework-interacting Cu^{II} species (fw-Cu^{II}). Among these, a low-temperature (LT) redox-active component (**PC3**) is found, efficiently undergoing reduction to Cu^{I} (**PC2**) in inert atmosphere from 250 °C upwards. A LT redox-inert component is also identified (**PC5**): it remains stable in He up to 400 °C and is more abundantly formed in the highly active 0.18Cu-HMOR(7) material.

The characteristic XANES features of the theoretical spectra, together with their temperature-dependent dynamics, provide the basis for their assignment, as detailed in the caption of Figure 3. MCR analysis reveals two fw-Cu^{II} species, characterized by different resistance towards self-reduction, and distinct XANES features. One type of fw-Cu^{II} is found to efficiently reduce to Cu^{I} already at 250 °C in He (low-temperature (LT) redox-active fw-Cu^{II}, PC3 in Figure 3b,c). In contrast, the species referred to as LT redox-inert fw-Cu^{II} (PC5 in Figure 3b,c), remains stable until 400 °C in inert atmosphere. This behaviour is consistent with the higher stability predicted for multimeric Cu-oxo cores,[49] with respect to monomeric Cu^{II} species. The latter could include $[Cu^{II}OH]^+$, $[Cu^{II}O]^+$, and, in the presence of O_2, $[Cu^{II}O_2]^+$ formed at a single-Al docking site during dehydration.

LT redox-inert fw-Cu^{II} is significantly more abundant in the highly productive 0.18Cu-HMOR(7). Its XANES is characterized by more intense and sharper peaks with respect to the LT redox-active component, especially in the WL region. LT redox-inert fw-Cu^{II} (PC5) is observed in both inert and oxidizing environments, which supports anaerobic pathways as a viable alternative to direct routes involving molecular oxygen activation at Cu sites. With this respect, the formation of dicopper(II) cores from the condensation of neighbouring $[CuOH]^+$ species (2 $[Cu^{II}OH]^+ \rightarrow [Cu^{II}OCu^{II}]^{2+} + H_2O$), amply proposed in the previous literature,[20, 40, 50] could represent a plausible hypothesis. Nonetheless, during a prolonged activation at 500 °C, an oxidizing environment appears necessary for its stabilization, in agreement with O_2 temperature-programmed desorption results for Cu-ZSM-5.[51] Replicating the

inert pre-treatment conditions for the MTM reaction cycle over selected Cu-MOR samples resulted in a drastic productivity loss (see SI, Section S6). Under these conditions, the normalized productivity drops to 0.021 and 0.007 mol CH_3OH/mol Cu for 0.18Cu-HMOR(7) and 0.36Cu-HMOR(11), respectively, still pointing towards a higher residual activity for 0.18Cu-HMOR(7). All these lines of evidence are consistent with the *operando* XAS results and indicate the LT redox-inert fw-Cu^{II} (PC5 in Figure 3) as the active site for the MTM conversion over Cu-MOR. We should note that what is here referred to as 'the active site' most likely consists into a molecular-level distribution of Cu-species (e.g. in correspondence of different Al positions in the framework[23]) giving similar MTM activity and lumping into the same principle component in MCR-XANES analysis.

3.4 Quantitative evidences for a di-copper active site

We further characterized the same Cu-MOR materials investigated by *operando* XAS by collecting higher-quality HERFD XANES after the samples were kept at 500 °C in O_2 for 30 min. Using the 'pure' spectra in Figure 3b as references, we applied linear combination fit (LCF) analysis to these higher-quality spectra, to accurately determine Cu-speciation in the complete set of samples (Figure 4b,c, see also SI, Section S9). Under these conditions, the outperforming 0.18Cu-HMOR(7) contains the highest fraction of LT redox-inert fw-Cu^{II} (PC5, 47% of total Cu). This is in contrast to the three other materials where the LT redox-active species is promoted: it accounts for 52-78% of total Cu, at the expense of our presumed active site (PC5, 18-24%). Minor contributions from the Cu^{II} dehydration intermediate species (PC4) are also detected in all the samples except for 0.36Cu-HMOR(11).

The duration of each reaction step clearly has a strong impact the performance of the tested materials (Figure 2e). Thus, we re-evaluated the four Cu-MOR zeolites under an *ad hoc* set of conditions (HERFD XANES testing conditions, Figure 4a). Here, the O_2-activation step is set to 30 min, as used in HERFD XANES experiments, whereas a 360-min-long CH_4 loading step is employed to efficiently saturate all the available active sites (see SI, Section S7). This ensures that the measured yield of C-containing products (CH_3OH and minor fractions of over-oxidation products) per Cu is a trustworthy measure of the fraction of active Cu formed during the O_2-activation step at these conditions. Figure 4d correlates the thus determined mol activated CH_4/mol Cu with the fraction of LT redox-inert fw-Cu^{II} (PC5) from LCF analysis. The experimental points for our Cu-MOR sample series after O_2-activation (full coloured circles in Figure 4d) accurately approximate the ideal trend line for stoichiometric MTM conversion over a di-copper AS (dark red line in Figure 4d), unambiguously demonstrating that two Cu ions are cooperatively involved in the activation of a CH_4 molecule over these materials. The same plot as in Figure 4d but reporting the mol CH_3OH/mol Cu *vs* fraction of PC5 can be found in SI (Section S10) together with some discussion about the process selectivity as a function of the AS abundance.

For the Si/Al = 7 Cu-MOR samples, we also investigated a different pre-treatment, exposing He-activated materials to O_2 at 500 °C (see SI, Table S5). The corresponding experimental points, obtained correlating results of HERFD XANES LCF analysis and productivity per Cu evaluated after the same pre-treatment, are reported as empty squares in Figure 4d. Thus, both for different materials and even when using different activation protocols for the same material, the points keep following the di-copper AS trend line, evidencing how the same dimeric active site is consistently conserved. Remarkably, a di-copper(II) AS is consistent with the results by Newton et al.,[48] supporting a mechanism based on the Cu^{I}/Cu^{II} redox couple rather than on the Cu^{II}/Cu^{III} one, or alternative routes involving Cu^{II}–O• radicals.

The pure HERFD XANES signature of PC5 and the structural insights from *operando* EXAFS both indicate that the Cu_2O_x AS is built up by three-fold O-ligated Cu^{II} units, in a coordination motif fully consistent with the available models of the mono(μ-oxo) dicopper(II) core in Cu-zeolites.[10, 19, 23, 47] (Figure 4e) Nonetheless, based on our XAS results, a trans-(μ-1,2-peroxo) dicopper(II) core (Figure 4f), as recently proposed in Cu-CHA,[52] cannot be ruled out. Having established the AS as a di-copper(II) species discourages the direct involvement of mononuclear $[Cu(OH)]^+$ complexes stabilized in the proximity of an isolated 1-Al site, although these species would possess a tridentate geometry analogue to the one of the Cu_2O_x moieties depicted in Figure 4e,f. As previously proposed for Cu-CHA,[16] $[Cu(OH)]^+$ species most likely serve as precursors to form the active Cu_2O_x species, through processess favoured by activation at high temperature. Reasonably, based on our previous XANES-MCR results about Cu-

speciation in Cu-CHA,[43] it is plausible to connect $[Cu(OH)]^+$ with the PC3 component (LT redox-active fw-Cu^{II}) found here for Cu-MOR. Overall, the fundamental knowledge accessed here will pave the way to future research aiming to assess in detail the identity of the di-copper AS in Cu-MOR.

Projecting the normalized yield obtained at the reference testing conditions (480 min-long O_2-activation) for 0.18Cu-HMOR(7) on the spectroscopically-validated di-copper AS trend line, we estimate more than 90% of total Cu to be coordinated in Cu_2O_x active species, resulting in the highest productivity per Cu reported to date for MTM over Cu-exchanged zeolites. Hence, prolonged exposure to O_2 at 500 °C promotes important reorganization phenomena in the Cu ions siting, resulting in the dynamic transformation of inactive Cu into active species (or possibly precursor to active species). In the presence of the most favourable compositional landscape, such as in 0.18Cu-HMOR(7), these processes finally yield a *quasi-single-site* catalyst, where virtually all Cu is organized into active Cu_2O_x cores

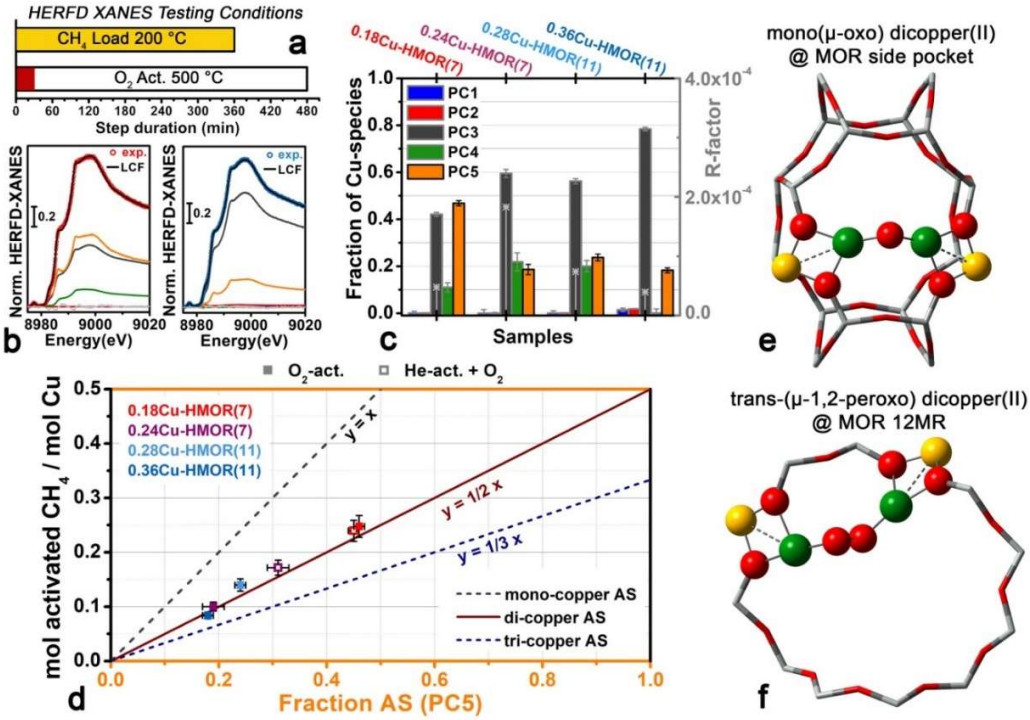

Figure 4. a, Bar plot representing the duration of the O_2-activation and CH_4 loading steps at the HERFD XANES testing conditions, adopted into parallel laboratory tests to effectively correlate spectroscopy results and performance. **b,** Comparison between experimental HERFD XANES of representative O_2-activated Cu-MOR samples, namely 0.18Cu-HMOR(7) and 0.36Cu-HMOR(11), with the correspondent best-fit curves from LCF analysis, using the 'pure' spectra from MCR analysis (Figure 3b) as references. For each fitted spectrum, the LCF components scaled by their respective optimized weights, and the LCF residuals are reported (the same information for the whole set of samples can be found in the SI, Section S9). **c,** Cu-speciation in the O_2-activated Cu-MOR series as determined from LCF analysis of HERFD XANES spectra. The Cu-species (PC1-PC5) are denoted using the same colour code as used in Figure 3b,c. The LCF R-factor is also reported (grey stars, right ordinate axis). **d**, Quantitative correlation between the normalized productivity evaluated at the HERFD XANES testing conditions and the fraction of LT redox-inert fw-Cu^{II} (PC5 – our presumed AS) from LCF analysis (O_2-activation: full coloured symbols; He-activation + O_2: empty coloured symbols). All the experimentally-determined values match the ideal trend line for stoichiometric conversion over a di-copper AS, reported as a full dark red line. **e-f,** Illustrations of possible Cu_2O_x AS in the MOR framework compatible with the experimental results reported here, namely (**e**) a mono(μ-oxo) dicopper(II) core in the MOR side pocket and (**f**) a trans-(μ-1,2-peroxo) dicopper(II) core in the MOR 12MR. Atom color code: Cu, green; O, red; Si, grey; Al, yellow.

4. Conclusions

This study provides a novel perspective on the complex nature and dynamics of Cu ions in the MOR framework and explores the impact of these factors on the MTM conversion. Compositional characteristics (Cu/Al and Si/Al ratios) appear to determine an upper threshold for the productivity of the materials. An optimum combination of framework Al distribution (influenced by synthesis parameters and Si/Al ratio) with Cu-loading is shown to exist, enabling uniquely high activity for methane activation, as seen for 0.18Cu-HMOR(7). However, productivity in Cu-MOR can be further modulated by adjusting the process conditions. Synergizing the most favourable synthesis and compositional parameters and reaction conditions, we obtained the highest methanol yield per Cu yet reported for MTM over Cu-zeolites, of 0.47 mol/mol.

Conventional XAS under *operando* conditions evidenced specific fingerprints of the AS, revealing that both active and inactive fw-Cu^{II} species coexist after O_2-activation. Enhancing the spectroscopic contrast by MCR analysis of HERFD XANES data, we captured the XANES signature of each Cu-species present in the MOR framework. This approach enabled an accurate quantification of Cu-speciation in the activated materials. O_2-activation and CH_4 loading time were observed to drastically impact the yield. Thus, we adopted consistent protocols for both spectroscopy and testing to quantitatively correlate Cu-speciation to productivity per Cu. Furthermore, we linked a specific fw-Cu^{II} moiety with the MTM AS (or 'pool' of ASs), characterized by a higher resistance toward self-reduction and mostly favoured in 0.18Cu-HMOR(7). We directly correlated the abundance of such Cu^{II} species to the yield of CH_4 oxidation products per Cu, over several combinations of compositional and pre-treatment parameters. For the first time, the fraction of active Cu in Cu-MOR has been quantified by a spectroscopic method and correlated with performance at relevant conditions, to provide quantitative evidence of the active site nuclearity.

Taken together, our results demonstrate that the active site for selective methane oxidation over Cu-mordenite is a di-copper site. This is based on two strong observations. First, we have prepared a material that activates nearly one methane molecule per two Cu. Second, we show that across a series of materials and activation protocols, the productivity increases with a slope of exactly 0.5 when the spectroscopically-determined concentration of *active* Cu is increased. The dynamics directing the speciation of Cu along activation, in combination with the highly active material described, suggest a clear direction for future research in the field.

ASSOCIATED CONTENT

Supporting Information.

The Supporting Information is available free of charge via the Internet at http://pubs.acs.org

Physico-chemical characterization, Additional experimental protocols and activity measuremetns, Details on *operando* XAS measurements, Additional information on MCR-ALS and LCF analyses.

AUTHOR INFORMATION

Corresponding Author

*stian.svelle@kjemi.uio.no

*pabb@topsoe.com

*elisa.borfecchia@unito.it

Present Addresses

‡ Universitat Stuttgart, Pfaffenwaldring 55, 70174 Stuttgart, Germany

† Center for Materials Science and Nanotechnology (SMN), Department of Chemistry, University of Oslo, 1033 Blindern, 0315 Oslo, Norway

Notes

The authors declare no competing financial interest

ACKNOWLEDGMENTS

This publication forms a part of the iCSI (industrial Catalysis Science and Innovation) Centre for Research-based Innovation, which receives financial support from the Research Council of Norway under contract no. 237922. EB acknowledges Innovation Fund Denmark (Industrial postdoc n. 5190-00018B). CL and AM acknowledge the Mega-grant of the Russian Federation Government to support scientific research at the Southern Federal University, No. 14.Y26.31.0001. We are grateful to W. van Beek for the competent support during our XAS experiments at the BM31 beamline of ESRF. D. S. Wragg, M. Signorile, E. S. Gutterød and A. Lazzarini are acknowledged for support in the materials' characterization and testing. K. P. Lillerud is acknowledged for insightful discussions and advice on the chemistry of the studied materials.

REFERENCES

1. Schwach, P.; Pan, X. L.; Bao, X. H., *Chem. Rev.* **2017,** *117*, 8497-8520.
2. Tomkins, P.; Ranocchiari, M.; van Bokhoven, J. A., *Acc. Chem. Res.* **2017,** *50*, 418-425.
3. Horn, R.; Schlögl, R., *Catal. Lett.* **2015,** *145*, 23-39.
4. Arutyunov, V., *Catal. Today* **2013,** *215*, 243-250.
5. Ravi, M.; Ranocchiari, M.; van Bokhoven, J. A., *Angew. Chem.-Int. Edit.* **2017,** *56*, 16464-16483.
6. Balasubramanian, R.; Smith, S. M.; Rawat, S.; Yatsunyk, L. A.; Stemmler, T. L.; Rosenzweig, A. C., *Nature* **2010,** *465*, 115-119.
7. Groothaert, M. H.; Smeets, P. J.; Sels, B. F.; Jacobs, P. A.; Schoonheydt, R. A., *J. Am. Chem. Soc.* **2005,** *127*, 1394-1395.
8. Snyder, B. E. R.; Bols, M. L.; Schoonheydt, R. A.; Sels, B. F.; Solomon, E. I., *Chem. Rev.* **2018,** *118*, 2718-2768.
9. Sushkevich, V. L.; Palagin, D.; Ranocchiari, M.; van Bokhoven, J. A., *Science* **2017,** *356*, 523-527.
10. Woertink, J. S.; Smeets, P. J.; Groothaert, M. H.; Vance, M. A.; Sels, B. F.; Schoonheydt, R. A.; Solomon, E. I., *P. Natl. Acad. Sci. USA.* **2009,** *106*, 18908-18913.
11. Alayon, E. M.; Nachtegaal, M.; Ranocchiari, M.; van Bokhoven, J. A., *Chem. Commun.* **2012,** *48*, 404-406.
12. Grundner, S.; Luo, W.; Sanchez-Sanchez, M.; Lercher, J. A., *Chem. Commun.* **2016,** *52*, 2553-2556.
13. Grundner, S.; Markovits, M. A.; Li, G.; Tromp, M.; Pidko, E. A.; Hensen, E. J.; Jentys, A.; Sanchez-Sanchez, M.; Lercher, J. A., *Nat. Commun.* **2015,** *6*, 7546.
14. Tomkins, P.; Mansouri, A.; Bozbag, S. E.; Krumeich, F.; Park, M. B.; Alayon, E. M.; Ranocchiari, M.; van Bokhoven, J. A., *Angew. Chem.-Int. Ed.* **2016,** *55*, 5467-5471.
15. Wulfers, M. J.; Teketel, S.; Ipek, B.; Lobo, R. F., *Chem. Commun.* **2015,** *51*, 4447-4450.
16. Pappas, D. K.; Borfecchia, E.; Dyballa, M.; Pankin, I. A.; Lomachenko, K. A.; Martini, A.; Signorile, M.; Teketel, S.; Arstad, B.; Berlier, G.; Lamberti, C.; Bordiga, S.; Olsbye, U.; Lillerud, K. P.; Svelle, S.; Beato, P., *J. Am. Chem. Soc.* **2017,** *139*, 14961-14975.
17. Latimer, A. A.; Kulkarni, A. R.; Aljama, H.; Montoya, J. H.; Yoo, J. S.; Tsai, C.; Abild-Pedersen, F.; Studt, F.; Norskov, J. K., *Nat. Mater.* **2017,** *16*, 225-229.
18. Palagin, D.; Knorpp, A. J.; Pinar, A. B.; Ranocchiari, M.; van Bokhoven, J. A., *Nanoscale* **2017,** *9*, 1144-1153.
19. Vanelderen, P.; Snyder, B. E.; Tsai, M. L.; Hadt, R. G.; Vancauwenbergh, J.; Coussens, O.; Schoonheydt, R. A.; Sels, B. F.; Solomon, E. I., *J. Am. Chem. Soc.* **2015,** *137*, 6383-6392.
20. Alayon, E. M.; Nachtegaal, M.; Bodi, A.; Ranocchiari, M.; van Bokhoven, J. A., *Phys. Chem. Chem. Phys.* **2015,** *17*, 7681-7693.
21. Alayon, E. M. C.; Nachtegaal, M.; Bodi, A.; van Bokhoven, J. A., *ACS Catal.* **2014,** *4*, 16-22.
22. Bozbag, S. E.; Alayon, E. M. C.; Pecháček, J.; Nachtegaal, M.; Ranocchiari, M.; van Bokhoven, J. A., *Catal. Sci. Technol.* **2016,** *6*, 5011-5022.

23. Snyder, B. E. R.; Vanelderen, P.; Schoonheydt, R. A.; Sels, B. F.; Solomon, E. I., *J. Am. Chem. Soc.* **2018,** *140*, 9236-9243.
24. Sushkevich, V. L.; Palagin, D.; van Bokhoven, J. A., *Angew. Chem.-Int. Edit.* **2018,** *57*, 8906-8910.
25. Paolucci, C.; Parekh, A. A.; Khurana, I.; Di Iorio, J. R.; Li, H.; Albarracin Caballero, J. D.; Shih, A. J.; Anggara, T.; Delgass, W. N.; Miller, J. T.; Ribeiro, F. H.; Gounder, R.; Schneider, W. F., *J. Am. Chem. Soc.* **2016,** *138*, 6028-6048.
26. Paolucci, C.; Khurana, I.; Parekh, A. A.; Li, S. C.; Shih, A. J.; Li, H.; Di Iorio, J. R.; Albarracin-Caballero, J. D.; Yezerets, A.; Miller, J. T.; Delgass, W. N.; Ribeiro, F. H.; Schneider, W. F.; Gounder, R., *Science* **2017,** *357*, 898-903.
27. Ravel, B.; Newville, M., *J. Synchrotron Radiat.* **2005,** *12*, 537-541.
28. Bellet, D.; Gorges, B.; Dallery, A.; Bernard, P.; Pereiro, E.; Baruchel, J., *J. Appl. Crystallogr.* **2003,** *36*, 366-367.
29. Giordanino, F.; Borfecchia, E.; Lomachenko, K. A.; Lazzarini, A.; Agostini, G.; Gallo, E.; Soldatov, A. V.; Beato, P.; Bordiga, S.; Lamberti, C., *J. Phys. Chem. Lett.* **2014,** *5*, 1552-1559.
30. Borfecchia, E.; Lomachenko, K. A.; Giordanino, F.; Falsig, H.; Beato, P.; Soldatov, A. V.; Bordiga, S.; Lamberti, C., *Chem. Sci.* **2015,** *6*, 548-563.
31. Ruckebusch, C., *Resolving Spectral Mixtures: With Applications from Ultrafast Time-Resolved Spectroscopy to Super-Resolution Imaging*. Elsevier: 2016; Vol. 30.
32. de Juan, A.; Tauler, R., *Anal. Chim. Acta* **2003,** *500*, 195-210.
33. Ruckebusch, C.; Blanchet, L., *Anal. Chim. Acta* **2013,** *765*, 28-36.
34. Malinowski, E. R., *Factor analysis in chemistry*. Jon Wiley & Sons: New York, 2002.
35. Jaumot, J.; Gargallo, R.; de Juan, A.; Tauler, R., *Chemometrics Intell. Lab. Syst.* **2005,** *76*, 101-110.
36. Windig, W.; Guilment, J., *Anal. Chem.* **1991,** *63*, 1425-1432.
37. Bro, R.; De Jong, S., *J. Chemometr.* **1997,** *11*, 393-401.
38. Kim, Y.; Kim, T. Y.; Lee, H.; Yi, J., *Chem. Commun.* **2017,** *53*, 4116-4119.
39. Groothaert, M. H.; van Bokhoven, J. A.; Battiston, A. A.; Weckhuysen, B. M.; Schoonheydt, R. A., *J. Am. Chem. Soc.* **2003,** *125*, 7629-7640.
40. Larsen, S. C.; Aylor, A.; Bell, A. T.; Reimer, J. A., *J. Phys. Chem.* **1994,** *98*, 11533-11540.
41. Llabrés i Xamena, F. X.; Fisicaro, P.; Berlier, G.; Zecchina, A.; Palomino, G. T.; Prestipino, C.; Bordiga, S.; Giamello, E.; Lamberti, C., *J. Phys. Chem. B* **2003,** *107*, 7036-7044.
42. Sushkevich, V. L.; van Bokhoven, J. A., *Chem. Commun.* **2018,** *54*, 7447-7450.
43. Martini, A.; Borfecchia, E.; Lomachenko, K. A.; Pankin, I. A.; Negri, C.; Berlier, G.; Beato, P.; Falsig, H.; Bordiga, S.; Lamberti, C., *Chem. Sci.* **2017,** *8*, 6836-6851.
44. Glatzel, P.; Bergmann, U., *Coord. Chem. Rev.* **2005,** *249*, 65-95.
45. Singh, J.; Lamberti, C.; van Bokhoven, J. A., *Chem. Soc. Rev.* **2010,** *39*, 4754-4766.
46. Solomon, E. I.; Heppner, D. E.; Johnston, E. M.; Ginsbach, J. W.; Cirera, J.; Qayyum, M.; Kieber-Emmons, M. T.; Kjaergaard, C. H.; Hadt, R. G.; Tian, L., *Chem. Rev.* **2014,** *114*, 3659-3853.
47. Tsai, M. L.; Hadt, R. G.; Vanelderen, P.; Sels, B. F.; Schoonheydt, R. A.; Solomon, E. I., *J. Am. Chem. Soc.* **2014,** *136*, 3522-3529.
48. Newton, M. A.; Knorpp, A. J.; Pinar, A. B.; Sushkevich, V. L.; Palagin, D.; van Bokhoven, J. A., *J. Am. Chem. Soc.* **2018,** *140*, 10090-10093.
49. Pidko, E. A.; Hensen, E. J. M.; van Santen, R. A., *Proc. R. Soc. A-Math. Phys. Eng. Sci.* **2012,** *468*, 2070-2086.
50. Palomino, G. T.; Fisicaro, P.; Bordiga, S.; Zecchina, A.; Giamello, E.; Lamberti, C., *J. Phys. Chem. B* **2000,** *104*, 4064-4073.
51. Smeets, P. J.; Hadt, R. G.; Woertink, J. S.; Vanelderen, P.; Schoonheydt, R. A.; Sels, B. F.; Solomon, E. I., *J. Am. Chem. Soc.* **2010,** *132*, 14736-14738.

52. Ipek, B.; Wulfers, M. J.; Kim, H.; Göltl, F.; Hermans, I.; Smith, J. P.; Booksh, K. S.; Brown, C. M.; Lobo, R. F., *ACS Catal.* **2017,** *7*, 4291-4303.